Appearance of the Retina With Full-Field Optical Coherence Tomography

Kate Grieve, Olivier Thouvenin, Abhishek Sengupta, Vincent M. Borderie, Michel Paques

Special Issue

Appearance of the Retina With Full-Field Optical Coherence Tomography

Kate Grieve,[1,2] Olivier Thouvenin,[3] Abhishek Sengupta,[2] Vincent M. Borderie,[1,2] and Michel Paques[1,2]

[1]Quinze Vingts National Ophthalmology Hospital, Paris, France
[2]Vision Institute, UPMC Université Paris 06, Paris, France
[3]Institut Langevin, Paris, France

Correspondence: Kate Grieve, Institut de la Vision, Centre Hospitalier National d'Ophtalmologie des Quinze-Vingts, 17 rue Moreau, 75012 Paris, France; kategrieve@gmail.com.

Submitted: December 11, 2015
Accepted: March 14, 2016

Citation: Grieve K, Thouvenin O, Sengupta A, Borderie VM, Paques M. Appearance of the retina with full-field optical coherence tomography. *Invest Ophthalmol Vis Sci*. 2016;57:OCT96–OCT104. DOI:10.1167/iovs.15-18856

Purpose. To interpret full-field optical coherence tomography (FFOCT) images of ex vivo retina.

Methods. Flatmounted retinas of human, primate, pig, sheep, rat, and mouse were imaged using FFOCT. To identify retinal ganglion and amacrine cells, fixed samples immunolabeled against Tuj1 and Brn3a or live samples labeled in vitro with green fluorescent protein (GFP) were analyzed by combining FFOCT, fluorescence confocal microscopy (FCM), and fluorescence-FFOCT. To investigate postmortem tissue changes, time series were acquired over 48 hours and on fresh versus fixed tissue.

Results. With FFOCT, cell types and features such as nerve fiber bundles and RGC somas were resolved without use of contrast agents at 1-μm xyz resolution. Cell somas in the ganglion cell layer (GCL) in large mammals appeared predominantly bright with dark contours, while in rodents, GCL somas appeared dark with bright contours. RGC axon to soma junctions could be traced in the three-dimensional (3D) image stacks. Time series revealed undulation of retinal tissue samples over 48 hours, though no degradation of individual cells was detected, while paraformaldehyde fixation caused increased scattering and shrinkage.

Conclusions. Full-field OCT reveals micrometric morphologic detail in the retina without the use of contrast agents. We observed interspecies differences in optical properties of GCL somas. Fixation significantly alters retinal transparency hence reducing the visibility of microscopic features.

Keywords: imaging, optical coherence tomography, microscopy, retina, explant

Full-field optical coherence tomography or microscopy (FFOCT or FFOCM)[1,2] is a variant of optical coherence tomography (OCT)[3] that has developed over the past decade to provide cellular-resolution images of ex vivo tissue specimens in depth without the use of contrast agents. It has been used for imaging of the retina,[4] cornea,[5–7] corneal limbus,[8] and other ophthalmic tissues, along with other biological tissues such as brain,[9] breast,[10,11] and gastrointestinal tissues.[12]

The lack of the need for fixation and contrast agents in FFOCT is an advantage, particularly in longitudinal studies where a single retinal explant, for example, is to be imaged at multiple timepoints. However, to remove ambiguity in the identification of features seen in FFOCT, correlation with images of the same tissues using other techniques is necessary. Fluorescence confocal microscopy (FCM) using fluorescent markers allows identification of different cell types, axons, and vasculature. Fluorescence-FFOCT provides precise overlay of fluorescence and FFOCT images captured in one multimodal instrument. The current study sought to correlate FFOCT images with FCM and fluorescence-FFOCT images in order to identify the retinal features seen with FFOCT, and to monitor changes in these features over time and after fixation.

Methods

Tissues

Human Tissues. Human ocular globes from donors were obtained from the Surgery School (Ecole de Chirurgie, Assistance Publique Hôpitaux de Paris, Paris, France) via a protocol approved by the institutional review boards of the Surgery School and the Quinze Vingts National Ophthalmology Hospital (CPP Ile-de-France V, Paris, France). Globes were removed from cadavers less than 48 hours postmortem and transported in CO_2-free medium (Gibco, Life Technologies, Warrington, UK) from the Surgery School to the Quinze Vingts National Ophthalmology Hospital where they were dissected to isolate the retina for imaging. Dissected retinas were imaged fresh, immersed in neurobasal-A medium (Gibco, Life Technologies). Five retinal specimens from five donors (average age 80, range, 63–95) were examined. Specimens one and two were small samples from peripheral retinal locations, specimen three surrounded the optic nerve, and specimens four and five were wide bands of tissue that included the macula and optic nerve. Samples were dissected to a flatmount directly in the FFOCT sample holder (i.e., freely floating rather than adhered to a glass

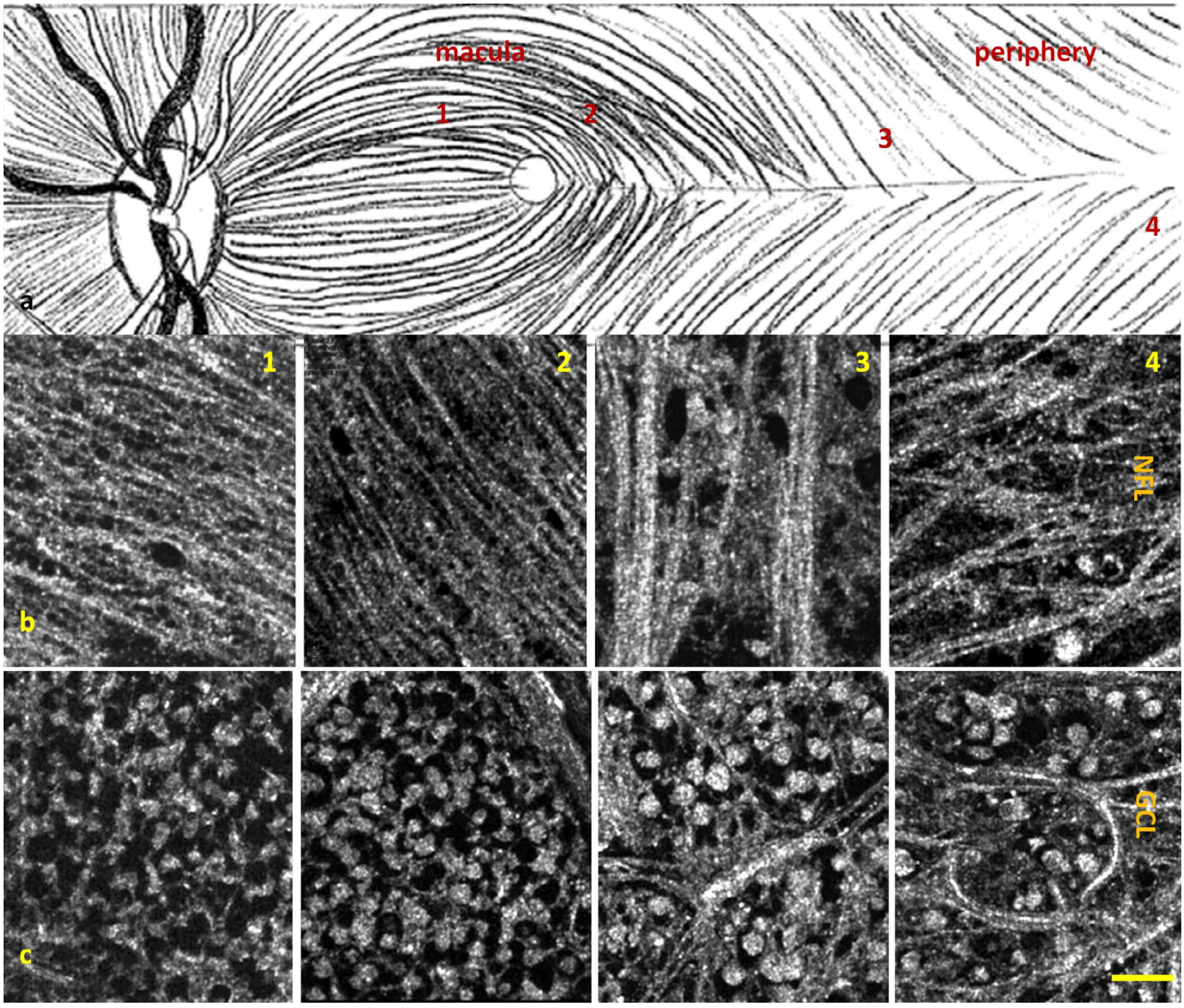

FIGURE 1. Median raphe in human. Full-field OCT images of human retina, in subject two. (**a**) Illustration of fundus showing raphe median region running from macula to periphery. One through four indicate approximate zones of en face images in row (**b**) NFL; row (**c**) GCL. *Scale bar*: 50 μm.

or membrane support) and gently immobilized under coverslip for imaging.

Animals and Animal Tissues. All animal manipulation was approved by the Quinze Vingts National Ophthalmology Hospital and regional review board (CPP Ile-de-France V), and was performed in accordance with the ARVO Statement for the Use of Animals in Ophthalmic and Vision Research.

Nine pig and four sheep ocular globes were obtained from a private research facility and transported in PBS to the Vision Institute. Six primate ocular globes were obtained from a partner research facility and transported to the Vision Institute in CO2-free neurobasal medium inside a device that maintained oxygenation. Two rat (Long-Evans; Janvier Labs, Le Genest Saint Isle, France) and 14 mouse (C57 BL/6, Balb/c albino, and Auburn; Janvier Labs) eyes were obtained from the animal facility of the Vision Institute. Anterior segments were removed and either the full thickness retina was imaged with the retinal pigment epithelium (RPE) and choroid intact, or the retinas were dissected at the level of the photoreceptor outer segments so that the RPE and choroid were excluded from the images. Retinal samples were flatmounted either directly in the FFOCT sample holder, or adhered to a membrane support for transfer to the FFOCT sample holder, immersed in CO2 – free neurobasal medium, and gently immobilized under coverslip for FFOCT imaging.

Imaging Technologies

Full-Field Optical Coherence Tomography. Full-field OCT[1,2] is a variant of conventional OCT[3] in which two-dimensional (2D) en face images are captured on a camera and three-dimensional (3D) data sets may be obtained by scanning in the depth direction. This configuration and the use of a white light source allow for higher axial and cross-sectional resolution than conventional OCT, on the order of 1 μm. No contrast agents are required as contrast is entirely endogenous. Full-field OCT can therefore perform micrometer resolution 3D imaging noninvasively in fresh or fixed ex vivo biological tissue samples. In retina, FFOCT enables imaging of fresh or fixed flat-mounted tissue at 1 μm^3 resolution (i.e., showing cellular details as in histology, but without slicing or staining tissue).

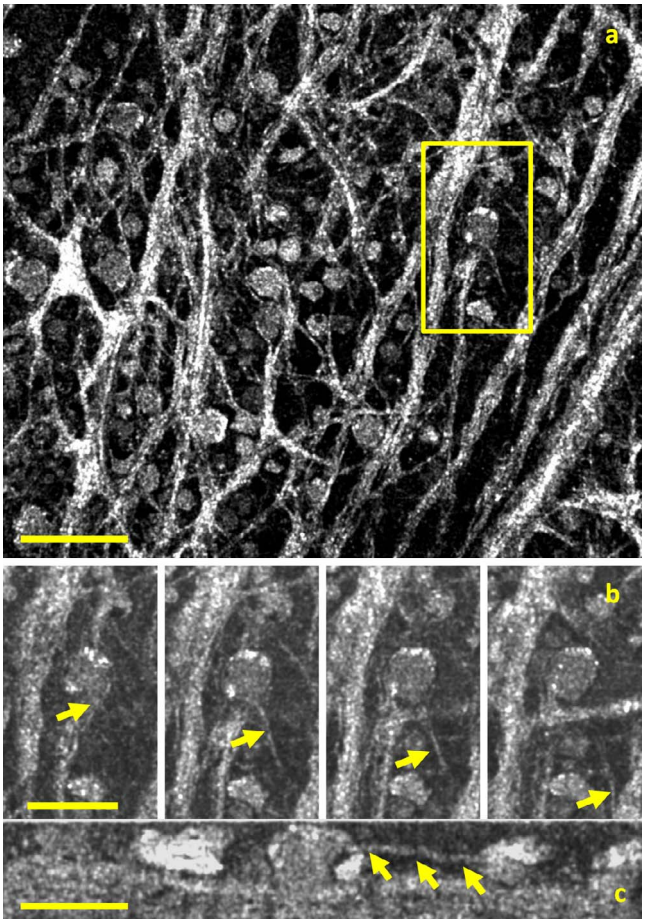

FIGURE 2. Human retinal ganglion cell axons and somas. (**a**) Wide-field en face view of human nerve fiber layer in subject two, *scale bar*: 500 μm. (**b**) Zooms on FFOCT images of an individual 2-μm thick axon (*arrows*) departing from a ganglion cell soma in en face views spaced in consecutive 2-μm depth steps, and (**c**) the cross-section of the same cell along the length of the axon. *Scale bars*: 50 μm. Supplementary Movie S1 shows tracing of axons in this subject in 3D.

The FFOCT system used in this study (LLTech, Paris, France) has been described previously.[7] Illumination is provided by a halogen source, whose short coherence length leads to an axial resolution of 1 μm. The full field is illuminated and images are captured on a complementary metal oxide semiconductor (CMOS) camera. The interferometer arms hold a matched pair of microscope objectives in the Linnik configuration. Water immersion at ×10 objectives with 0.3 numerical aperture lead to a lateral resolution of 1.6 μm. Penetration depth depends on tissue content and transparency and is approximately 200 μm in retina. Wide-field images can be displayed by automated montaging to image samples up to 25 mm in diameter, or stacks of images in depth can be captured. A 2 × 2 mm^2 montaged field is captured in less than five minutes, and a 200 μm × 1 mm × 1 mm 3D stack is also captured in less than 5 minutes.

Fluorescence Confocal Microscopy. Fluorescence confocal microscopy provides microscopic views of fluorescently labeled features within tissue. A laser-scanning FCM (Fluoview FV1200; Olympus, Rungis, France) was used to image fluorescently-labeled human retinal specimens. Image stacks covering 100-μm depth in 20 steps were acquired at regions of interest on labeled specimens flatmounted between slide and coverslip, with a ×10 objective.

Fluorescence-FFOCT. While FFOCT shows tissue architecture thanks to its intrinsic contrast produced by backscattered light, and FCM provides information on specific cell types or labeled features, correlation of the two requires careful handling and positioning of the tissue during FFOCT imaging, followed by the fluorescent labeling and specimen mounting process, followed by FCM imaging, plus the time-consuming scanning required to map large zones in order to enable identification of macroscopic features that can be used as signposts to microscopic features. The multiple steps in these processes imply some degree of imprecision in the final correlation, as image overlay at the cell-to-cell level between two different microscopic techniques is extremely challenging. A desirable alternative is to use a multimodal imaging system that offers pixel-to-pixel colocalization on FFOCT and fluorescence channels. This was possible using a prototype multimodal fluorescence-FFOCT microscope developed recently at the Langevin Institute, Paris, France. Compared with previous fluorescence-FFOCT setups,[13,14] in the set-up used here, fluorescence is acquired simultaneously with the FFOCT measurements, meaning image capture is faster. Briefly, this set-up operated in a similar fashion to conventional FFOCT but with the addition of a blue light emitting diode (LED; M470L2, 650 mW; Thorlabs, Newton, NJ, USA) centered at 470 nm, blocked by an excitation filter ($\lambda = 500$ nm, FES0500; Thorlabs) to excite fluorophores. The two illumination beams are combined and focused onto the sample, and in the detection path, FFOCT and fluorescence signals are separated by a Single Edge Dichroic Beamsplitter ($\lambda = 593$ nm, Di02-R594-22x27; BrightLine, Semrock, Rochester, NY, USA), and captured by two cameras, a CMOS (MV-D1024-160-CL-42; PhotonFocus, Lachen, Switzerland) for the FFOCT image and a scientific CMOS (5.5; PCO.edge; Kelheim, Germany) to capture the fluorescence image, with additional filters placed in front of the detection cameras to ensure independence of the two paths. As the optical path into the tissue is parallel for the FFOCT and fluorescence channels, an identical region of the sample is captured simultaneously on the FFOCT and fluorescence cameras. Numerical aperture (NA) 0.8 near infrared (NIR) water immersion microscope objectives at ×40 (Nikon, Paris, France) produced a field size of 220 × 220 μm and a pixel sampling of 210 nm per pixel. Full-field OCT image capture time is 3 ms, at a frame rate of 100 images per second. The fluorescence channel displays only one image, exposed for 500 ms.

Fluorescent Labeling

For FCM, retinal cell types were identified with a whole mount immunofluorescence assay. Briefly, after fixation with 4% PFA for 1 hour, the cells were permeabilized and blocked with 0.5% Triton X-100, 0.25% tween and PBS-BSA 5% for 1 hour at room temperature followed by incubation with combinations of the anti Tuj1 antibody (1:100; Chemicon, Billerica, MA, USA) and anti-Brn3a antibody (1:100; R&D Systems, Minneapolis, MN, USA) for one night at 4°C, and then with the secondary antibody (Alexa Fluor 488, 1:600) for 1 hour at room temperature, and nuclei were counterstained with 4′,6-diamidino-2-phenylindole (DAPI). One portion of each retinal specimen was incubated with PBS instead of the primary antibody to serve as a negative control.

For fluorescence-FFOCT, live macaque retinal cells were labeled in vitro by particle mediated acute gene transfer of green fluorescent protein (GFP). A Helios gene gun system (Bio-Rad, Hercules, CA, USA) was used for particle-mediated acute gene transfer in macaque retinal explants, similarly to what has been previously described.[15] Briefly, 10-mg gold microcarriers (1.6 μm; Bio-Rad) were coated with 20 μg of a

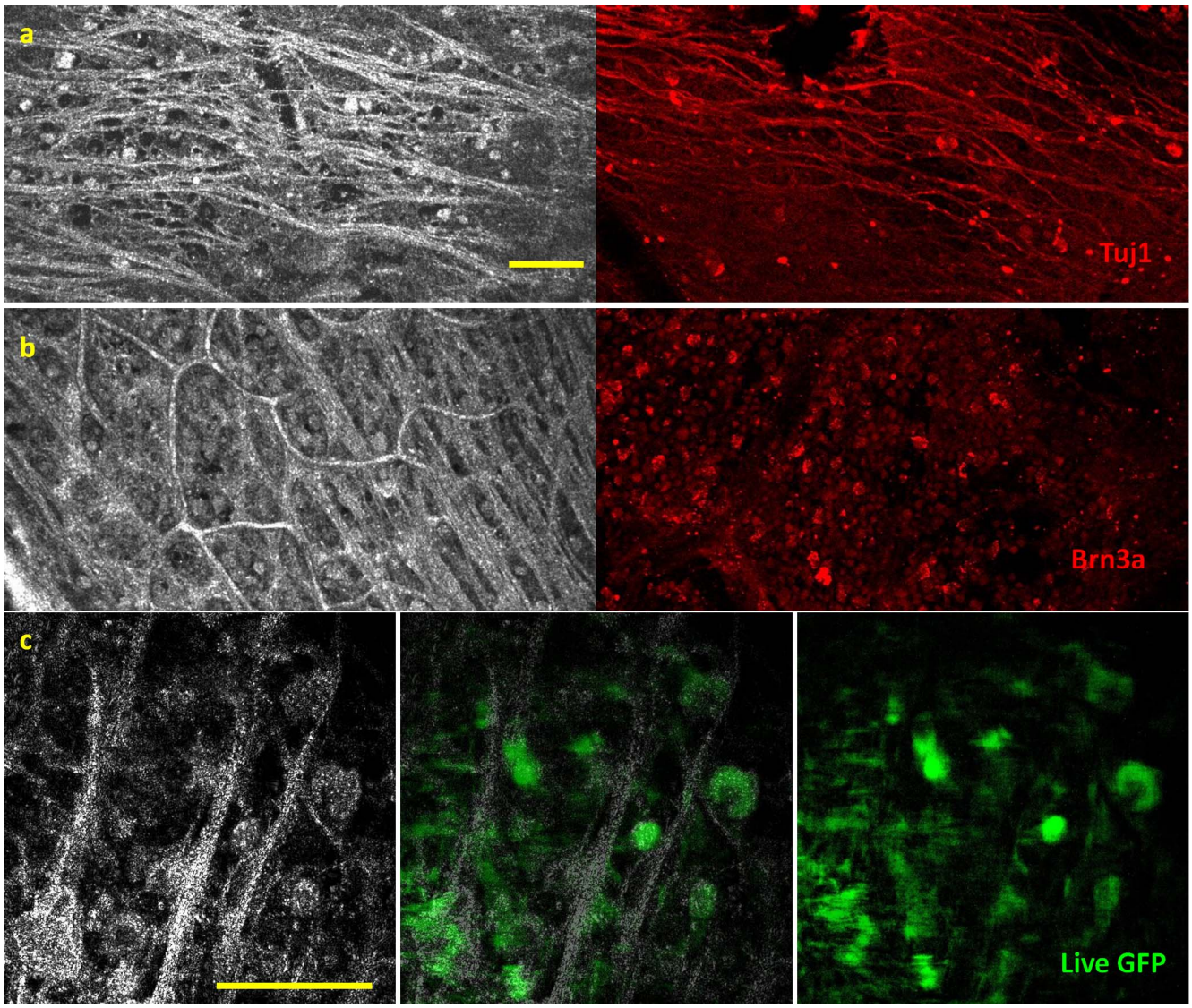

FIGURE 3. Full-field OCT and FCM in human and fluorescence-FFOCT in primate. (**a**, **b**) Full-field OCT (*left*) and FCM (*right*) images of human retina, in subject three. (**a**) Sparse axons and cells at periphery visible as hyperreflective structures in FFOCT (*left*) and similar region with FCM labeled with Tuj1 (*red*), which labels ganglion and amacrine cell somas and axons; (**b**) densely packed cells in GCL in location closer to optic nerve, where cells, nerve fibers and capillaries are visible as hyperreflective structures in FFOCT (*left*) and in similar region with FCM (*right*) where ganglion cell nuclei are labeled with Brn3a (*red*). (**c**) Full-field OCT (*left*) combined fluorescence-FFOCT (*center*) and fluorescence (*right*) images of GFP-labeled RGC somas in live macaque retina using fluorescence-FFOCT, with pixel to pixel overlay. *Scale bars*: 100 μm.

plasmid encoding CMV:CatCh-GFP in an AAV backbone in 3.2 mL ethanol solution and loaded into Tefzel tubing (Saint Gobain, Forge, PA, USA) using the gene gun Tubing Prep Station (Bio-Rad). The gene gun barrel was held 5 mm above the retinal explant (RGC side facing the barrel) and the plasmid bullets were propelled at a pressure of 110 psi. The explants were incubated at 37°C 5% CO_2 for 3 to 4 days post gene transfer.

Image Acquisition and Analysis

Qualitative Assessment of FFOCT Retinal Images. Full-field OCT en face images of retinal tissue specimens were analyzed for regions of interest. The orientation of the retinal tissue was deduced from wide field image montages and 3D image stacks, and the retinal location of each image stack was estimated based on the position of macroscopically recognizable features (e.g., optic nerve, macula), along with consideration of the microscopic features visible in the image stack (e.g., cell and axon density in relation to distance from optic nerve or macula, vessel structure). Based on these observations, tissues were dissected into smaller pieces for fluorescent labeling, with the combination of features labeled in each piece depending on the features considered most interesting in the FFOCT views.

Correlation of FFOCT With FCM and Fluorescence-FFOCT. Following fluorescent labeling, specimens were mounted between two coverslips on a microscope slide and positioned in the same orientations as they had been when part of the whole retina for FCM imaging. To search for similar microscopic zones, gross anatomical features such as vessels were used to approximately correlate image stack locations between FFOCT and FCM.

Fluorescence-FFOCT, with its colocalized fluorescence and FFOCT channels, automatically guaranteed precise correlation

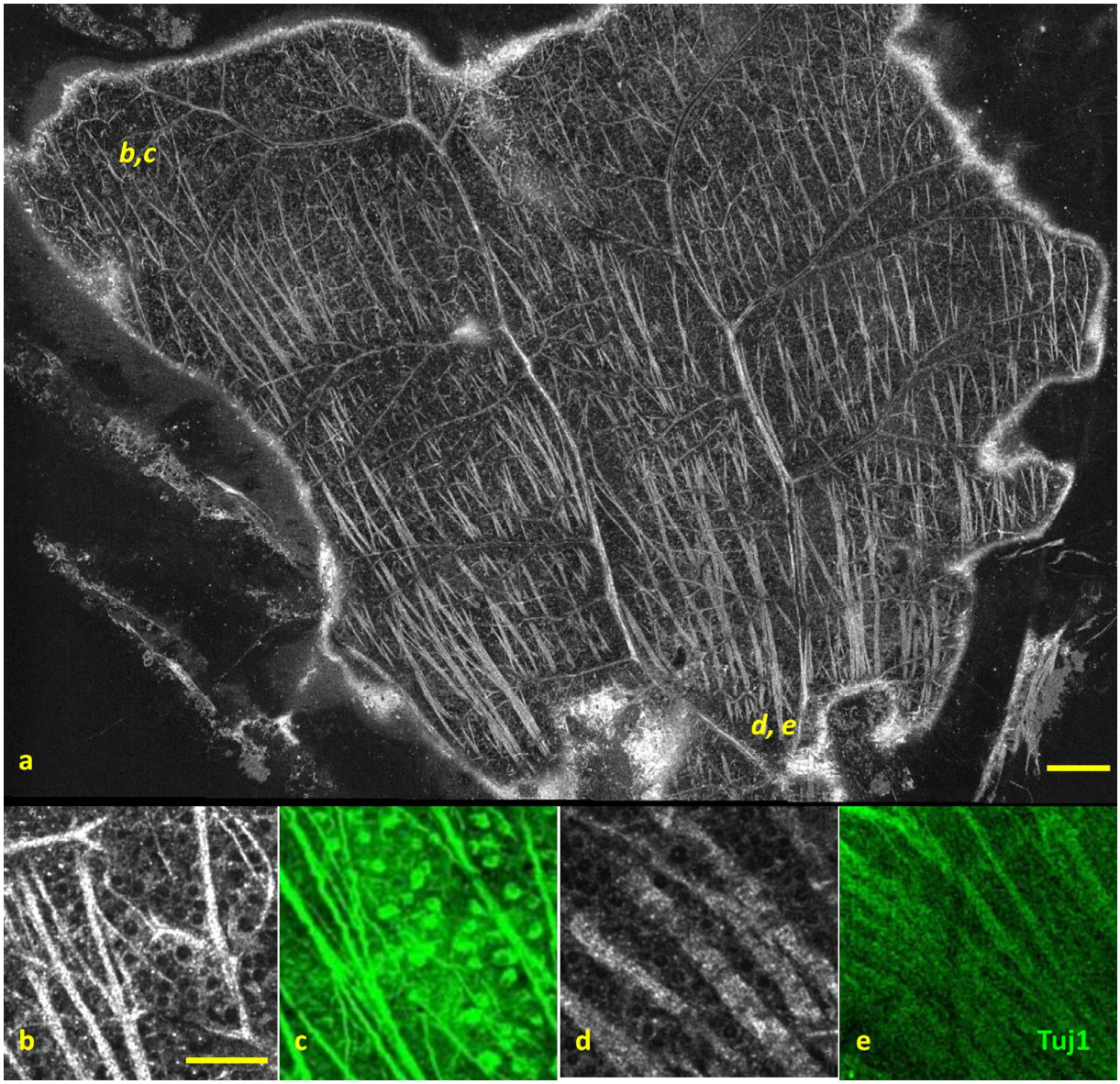

FIGURE 4. Rat retina in FFOCT and FCM. (**a**) Wide-field montage of flat-mounted section of rat retina with optic nerve located at the bottom of the image and the periphery at the *top*, with letters indicating locations of zoomed zones (**b**–**e**). (**b**) Zoom on peripheral zone with FFOCT and (**c**) similar zone in FCM with Tuj1 staining reveal axons and cells; (**d**) zoom on zone close to optic nerve with FFOCT, and (**e**) with FCM with Tuj1 staining reveal axon bundles. In FFOCT in rodent, axons are *bright* and cells are *dark centered, bright contoured. Scale bars*: (**a**) 200 μm, (**b**–**e**) 50 μm.

of the fluorescence and FFOCT signals to the scale of a single pixel.

Tissue Degradation In Time. Image stacks were acquired with FFOCT on three specimens of peripheral primate retina, hourly over a 48-hour period using automated image capture software (LLTech). Images at progressing time-points were compared qualitatively and intensity profiles at each time-point were plotted.

Tissue Changes Due to Fixation. Following imaging in fresh primate retina, a few drops of 4% paraformaldehyde (PFA) were added to the sample holder without displacing the retinal sample. Image stacks were acquired 30 minutes after addition of the fixative in identical locations to the stacks acquired when the tissue was fresh. Both qualitative and quantitative comparison of fresh versus fixed tissue was possible by considering image appearance, and by plotting intensity profiles of the resultant cross-sectional images to assess intensity, thickness and contrast changes between the fresh and fixed states.

RESULTS

Nerve Fiber and Retinal Ganglion Cell Layers

In human retina, axon bundles and cell bodies located in the ganglion cell layer (GCL) could be identified across the retina, and their differing distribution and density evaluated at different retinal locations. Figure 1 shows four image capture locations running from macula toward the periphery along an axis close to the median raphe, where dense axons and small densely packed cells around the macula gradually become sparser toward the periphery, with axons changing orientation corresponding to their positioning in relation to the median

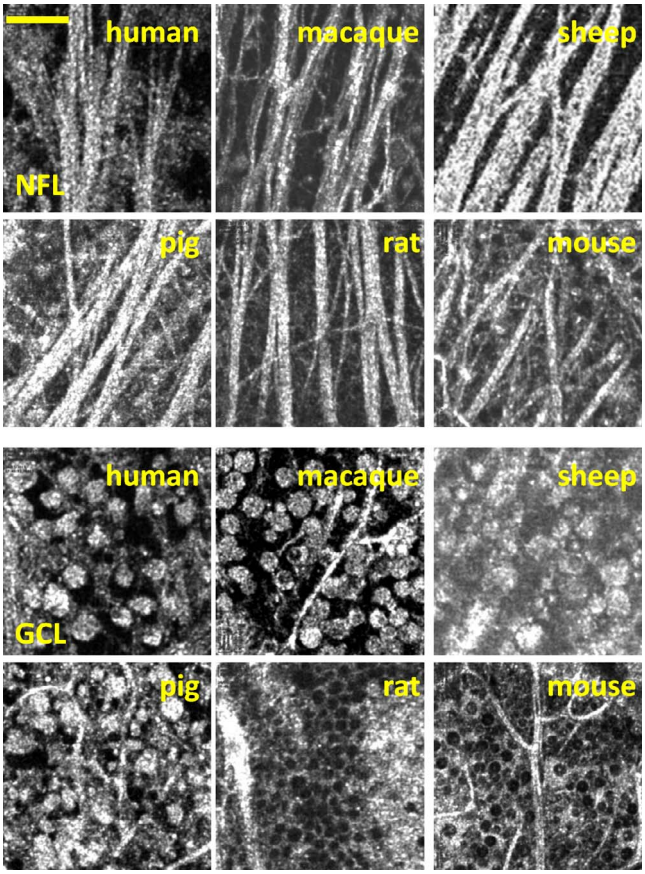

Figure 5. Nerve fiber layer and GCL interspecies variations. Full-field OCT images of human, primate, sheep, pig, mouse, and rat NFL (*six upper panels*) and GCL (*six lower panels*). Note contrast inversion on GCL somas between large mammals and rodents, which may be due to the differences in relative ganglion to amacrine cell populations between species (i.e., dark-centered cells may correspond to large-nuclei amacrines). *Scale bar*: 50 μm.

raphe and cell bodies becoming larger. Though nerve fiber and cell density can be evaluated from these images, identification of cell type as belonging to either the RGC or amacrine cell populations can only be confirmed by tracing a single axon to a soma which, due to its axon, can be positively identified as an RGC rather than amacrine cell. Individual axons departing from cell somas could be identified in FFOCT images in human, primate, pig, and sheep by zooming in on both en face and cross-sectional views (Fig. 2, Supplementary Movie S1), particularly when they detached from nerve fiber bundles. However, the diameter of single axons lies close to the resolution limit of FFOCT, meaning that they were hard to individually resolve when bundled. Identification of individual cell bodies is also time consuming, as it requires manual tracing of axons through the 3D image stacks (see Supplementary Movie S1).

An alternative method of identifying the cell bodies seen as RGC somas is the use of fluorescent labeling. This was performed either with FCM on similar zones of tissue samples that had been imaged fresh with FFOCT imaging then, or with fluorescence-FFOCT imaging on in vitro labeled samples to provide simultaneous, coincident acquisition of the FFOCT and fluorescence signals in a single overlay image.

Figures 3a and 3b present images in human retina acquired with FFOCT then susbsequent FCM on the same specimens in similar zones following immunohistochemical labeling, where Tuj1 positively labeled axons and ganglion and amacrine cell somas, (Fig. 3a) while Brn3a labeled only RGC nuclei (Fig. 3b). Figure 3c shows images acquired with fluorescence-FFOCT in macaque retina with in vitro GFP labeling of only RGC somas.

Figure 4 presents similar images in rat retina, with Tuj1 labeling identifying axons, ganglion and amacrine cells at two different retinal locations (Figs. 4c, 4e).

In human, primate, pig, and sheep, cell somas appeared as solid gray bodies (highly scattering) surrounded by dark (low scattering) contours, while in mouse and rat this contrast was inverted (dark bodies and bright contours; Fig. 5). In primate, some solid gray somas contained dark gray nuclei. As nuclear to cytoplasmic ratio is greater in amacrine cells[16] these cells containing visible nuclei may be displaced amacrine cells. Therefore, it follows that in the amacrine-dominant rodent retina,[17,18] we may be seeing mainly amacrine cells. Individual axons were too small to be resolved in mouse and rat, though axon bundles were seen as bright (highly scattering) structures in all species. Dendrites were not visible in any species, presumably as they are too small to be resolved.

Photoreceptor Layer

Figure 6 shows the photoreceptor layer, imaged photoreceptors facing upward, in primate. The rod and cone mosaic is clearly resolved with individual rods visible. In primate, the photoreceptor mosaic was also visible after traversing the retina from the nerve fiber layer side (Supplementary Movie S2). The photoreceptor mosaic was similarly resolved in the other large mammals, though not in rodents. This layer most frequently suffered damage during tissue dissection as the retinal tissue tends to naturally detach from the RPE at the photoreceptor level.

Tissue Degradation Over 48 Hours

Tissue became progressively more warped over 48 hours, causing local intensity variations in the cross-sectional image due to differences in proximity to the coverslip (i.e., zones at the peaks of undulations became brighter as closer to the light source, while troughs of undulations became relatively darker as more distant from the light source; Fig. 6). The photoreceptor mosaic was therefore less uniform in intensity, though patches close to the coverslip retained their initial appearance. Overall mean intensity was constant over time. No thickness changes were detected over the 48-hour time-period. Intensity increase over time at undulation peaks and decrease over time in undulation troughs caused overall contrast to become less uniform over time.

Fresh Versus Fixed Tissue

Qualitatively, visibility of individual photoreceptors, capillaries and vessels, nerve fibers and cells was reduced, and tissue appeared more homogeneous and dense in the fixed state with fewer discernible microscopic or celluar features (Fig. 6). Mean intensity increased by 28% ± 8% in the fixed versus fresh state ($P = 0.003$), with the most marked increase in intensity of the upper layers, to such an extent that deeper layers were far less visible than in the fresh tissue. On fixation, 20% ± 11% shrinkage of total retinal thickness was measured, with all of this shrinkage ($P = 0.007$) occurring in the photoreceptor layer (Fig. 7).

Discussion

Full-field OCT retinal imaging in several species reveals microscopic details that are not visible in conventional OCT,

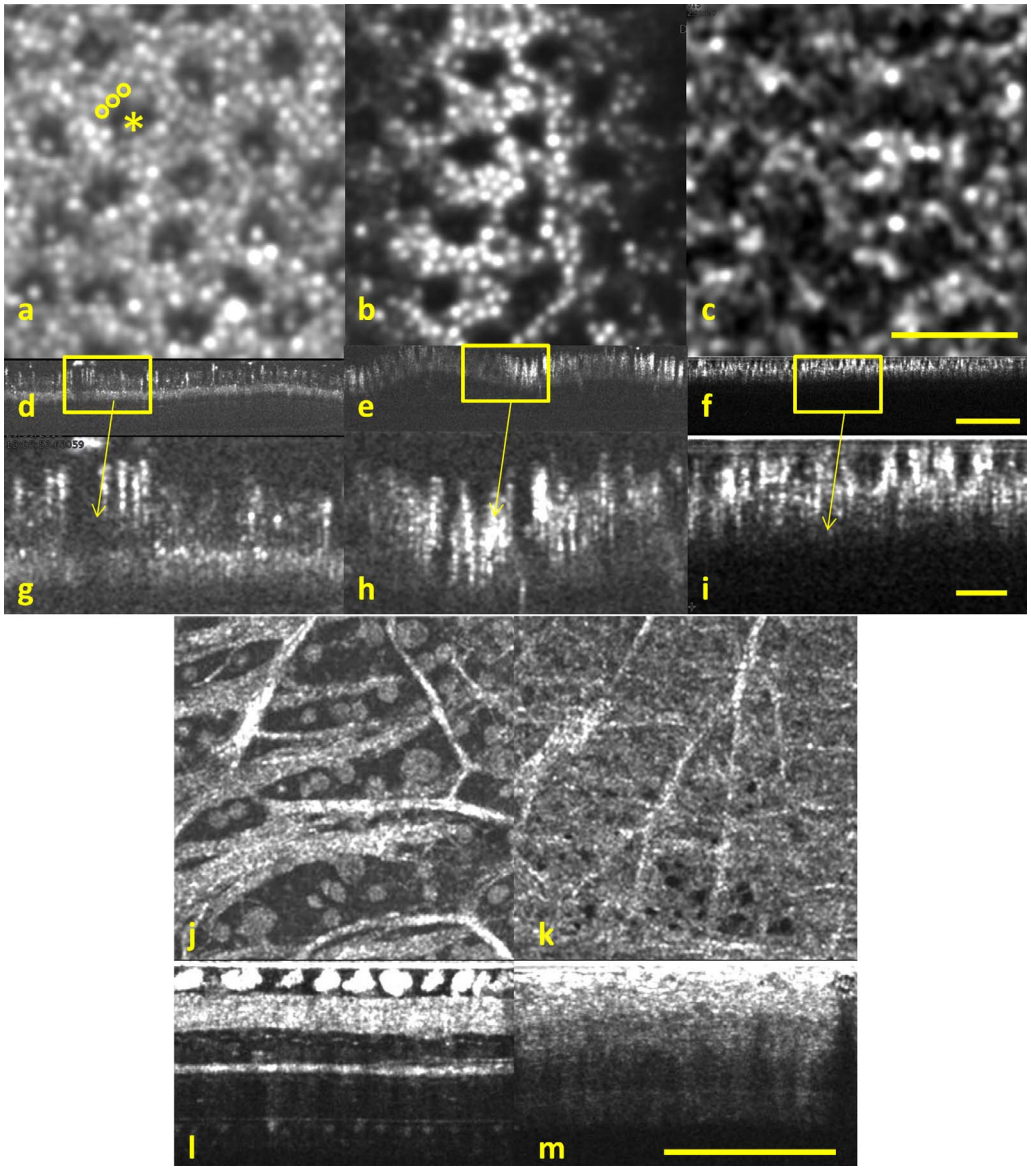

FIGURE 6. Time series and fresh versus fixed retina in primate. En face (**a**), cross-section (**d**), and zoomed cross-section (**g**) of the rod (*circles*) and cone (*asterisk*) photoreceptor mosaic 1 hour post dissection, imaged photoreceptors uppermost with FFOCT; (**b**, **e**, **h**) equivalent 48 hours post dissection; (**c**, **f**, **i**) equivalent fixed. Note that due to the waveguiding properties of photoreceptors, the sequence of layer contrasts in cross-section depends on which way up the tissue is placed. The sequence of layers as seen in conventional OCT[25,26] is recovered when imaged with nerve fibers uppermost. In this orientation, the nerve fiber bundles, vessels and ganglion cells are visible in fresh tissue (en face [**j**] and corresponding cross-section [**l**]), whereas the same tissue becomes homogeneous and highly scattering with few fibers visible when fixed (en face [**k**]) with reduced penetration in depth (corresponding cross-section [**m**]). *Scale bars*: (**a–c**) 20 μm, (**d–f**) 100 μm, (**g–i**) 20 μm, (**j–m**) 100 μm.

such as RGC axons and somas, other cell bodies and nuclei, capillaries, rods and cones. Being able to distinguish features in FFOCT and OCT images depends on the resolution ($1 \times 1 \times 1$ μm in FFOCT versus approximately $5 \times 15 \times 15$ μm in conventional OCT) but also the contrast of the structure, both intrinsically, and in relation to other structures within the image field. Hence, the visibility of new features in FFOCT is likely thanks to the superior resolution, though we acknowledge that contrast may be enhanced on certain features by postmortem changes to the scattering properties.

Full-field OCT imaging could be of interest for imaging of fresh tissues or explants of in vitro retina at different time points, because nerve fiber bundles and cell bodies are visible without the addition of contrast agents. However, in applications where identification of cell types is necessary, specific labeling is required, which may be achieved in vitro, as has been shown on primate retina (Fig. 3), or through immunohistochemical labeling on the fixed ex vivo tissues (Figs. 3, 4). A combination of FFOCT with subsequent FCM of similar zones in ex vivo tissues can provide evidence of cell types present, though precise simultaneous, coincident FFOCT and fluorescence image overlays can only be achieved with fluorescence-FFOCT. This imaging modality could prove useful in applications where information on both of specific fluorescence information and an overview of the surrounding tissue architecture is desired.

Should FFOCT be developed for in vivo retinal imaging, evaluation of nerve fiber bundle and cell density in the nerve fiber layer (NFL) and GCL could be useful in glaucoma diagnosis, where NFL thickness in OCT cross-sections is

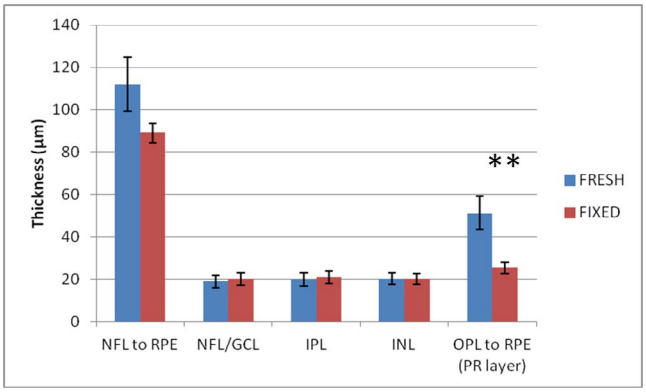

FIGURE 7. Fresh versus fixed layer thicknesses. Plot shows thickness of each layer and NFL to RPE in fresh versus fixed tissue, $^{**}P < 0.01$.

currently used as a surrogate indicator for GCL damage.[19,20] Full-field OCT could provide more precise measurement of this parameter, should in vivo retinal imaging with this technique become possible. In vivo FFOCT has been demonstrated in cornea[5] and skin, via endoscopy,[21] though has so far proved challenging for in vivo retinal imaging due to a lack of high-speed, large full-well depth camera technology, and high sensitivity to vibrations. However, an FFOCT setup destined for in vivo ophthalmic imaging is currently under development using a custom-developed CMOS camera (Quartz 2Mpx CoaXPress; Adimec, the Netherlands) and low-order aberration correction with a transmissive device.[22]

Where intact after dissection, the photoreceptor mosaic was resolved in the large mammals though less clearly in rodents, possibly due to the diameter of the cones in rodents being close to the resolution limit of the FFOCT system. The rod and cone mosaic in primate (Fig. 6) was of similar appearance to that seen with adaptive optics scanning laser ophthalmoscopy.[23] In primates, the photoreceptor mosaic could be resolved on imaging the retina both with photoreceptors uppermost, and with NFL uppermost (Supplementary Movie S2). This is promising for photoreceptor imaging in vitro with this technique, where the retina would be maintained in a physiological state with perfusion in the sample chamber, and the eye would be dissected to extract retinal explants with the RPE and choroid intact and attached.

We detected specimen warping over 48 hours, and surface scattering increase on fixation, leading to reduced penetration, which is consistent with the literature.[24] Visibility of axons and vessels in the en face direction was diminished in the fixed state, the photoreceptor mosaic became blurred and significant shrinkage occurred in the photoreceptor layer. This suggests that fixation causes tissue changes that may have an impact on interpretation of in vivo retinal features and layer appellations that rely on correlation with histology or electron microscopy.[25,26]

In conclusion, we have demonstrated the ability of FFOCT to detect and display images of features in retinal layers including the NFL and GCL, with resolution down to the single cell and single axon level, and the photoreceptor layer, with clear definition of individual rods and cones. Full-field OCT shows potential for precise imaging of the retina in fresh, in vitro or ex vivo tissue samples. We have shown that retinal thickness and mean scattering do not change over a 48-hour period, though the tissue tends to warp. In fixed retina, visibility of certain features is diminished, and retinal thickness changes are not uniform across layers, suggesting the need for caution in correlation of in vivo OCT cross-sections with histology, which may be of particular importance in the assignment of retinal layer appellations.

Acknowledgments

The authors thank Jens Duebel for use of the gene gun, Marie Darche, Sami Dalouz, Valérie Fontaine and Manu Simonutti for tissue preparation, Elisabeth Dubus and Serge Picaud for fluorescent labeling advice, and Djida Ghoubay for fluorescent labeling assistance.

Supported by grants from European Research Council SYNERGY Grant scheme (HELMHOLTZ, ERC Grant Agreement # 610110; European Research Council, Europe) and the Agence Nationale de Recherche (ANR), under a PRTS (Projet de Recherche Translationelle en Santé) Grant (ANR-13-PRTS-0009; Paris, France).

Disclosure: **K. Grieve**, None; **O. Thouvenin**, None; **A. Sengupta**, None; **V.M. Borderie**, None; **M. Paques**, None

References

1. Beaurepaire E, Boccara AC, Lebec M, Blanchot L, Saint-Jalmes H. Full-field optical coherence microscopy. *Opt Lett*. 1998;23:244–246.
2. Dubois A, Vabre L, Boccara AC, Beaurepaire E. High-resolution full-field optical coherence tomography with a Linnik microscope. *Appl Opt*. 2002;41:805–812.
3. Huang D, Swanson EA, Lin CP, et al. Optical coherence tomography. *Science*. 1991;254:1178–1181.
4. Grieve K, Paques M, Dubois A, Sahel J, Boccara C, Le Gargasson JF. Ocular tissue imaging using ultrahigh-resolution, full-field optical coherence tomography. *Invest Ophthalmol Vis Sci*. 2004;45:4126–4131.
5. Grieve K, Dubois A, Simonutti M, et al. In vivo anterior segment imaging in the rat eye with high speed white light full-field optical coherence tomography. *Opt Exp*. 2005;13:6286–6295.
6. Akiba M, Maeda N, Yumikake K, et al. Ultrahigh-resolution imaging of human donor cornea using full-field optical coherence tomography. *J Biomed Opt*. 2007;12:041202.
7. Ghouali W, Grieve K, Bellefqih S, et al. Full-field optical coherence tomography of human donor and pathological corneas. *Curr Eye Res*. 2015;40:526–534.
8. Grieve K, Ghoubay D, Georgeon C, et al. Three-dimensional structure of the mammalian limbal stem cell niche. *Exp Eye Res*. 2015;140:75–84.
9. Assayag O, Grieve K, Devaux B, et al. Imaging of non tumorous and tumorous human brain tissue with full-field optical coherence tomography. *Neuroimage Clin*. 2013;2:549–557.
10. Assayag O, Antoine M, Sigal-Zafrani B, et al. Large field, high resolution full field optical coherence tomography: a pre-clinical study of human breast tissue and cancer assessment. *Technol Cancer Res Treat Exp*. 2013;1:21–33.
11. Grieve K, Mouslem K, Assayag O, et al. Assessment of sentinel node biopsies with full-field optical coherence tomography. *Technol Cancer Res Treat*. 2016;15:266–274.
12. Grieve K, Palazzo L, Dalimier E, Vielh P, Fabre M. A feasibility study of full-field optical coherence tomography for rapid evaluation of EUS-guided microbiopsy specimens. *Gastrointest Endosc*. 2015;81:342–350.
13. Harms F, Dalimier E, Vermeulen P, et al. Multimodal full-field optical coherence tomography on biological tissue: toward all optical digital pathology. *Proceedings of Multimodal Biomedical Imaging VII*. San Francisco: Proc SPIE; 2012:21–26.
14. Auksorius E, Bromberg Y, Motiejunaite R, et al. Dual-modality fluorescence and full-field optical coherence microscopy for biomedical imaging applications. *Biomed Opt Exp*. 2012;3:661–667.

15. Moritoh S, Komatsu Y, Yamamori T, Koizumi A. Diversity of retinal ganglion cells identified by transient GFP transfection in organotypic tissue culture of adult marmoset monkey retina. *PLoS One*. 2013;8:e54667.
16. Curcio CA, Allen KA. Topography of ganglion cells in human retina. *J Comp Neurol*. 1990;300:5–25.
17. Smith CA, Chauhan BC. Imaging retinal ganglion cells: enabling experimental technology for clinical application. *Prog Retin Eye Res*. 2015;44:1–14.
18. Danias J, Shen F, Goldblum D, et al. Cytoarchitecture of the retinal ganglion cells in the rat. *Invest Ophthalmol Vis Sci*. 2002;43:587–594.
19. Chen C-L, Ishikawa H, Wollstein G, et al. Individual A-scan signal normalization between two spectral domain optical coherence tomography devices. *Invest Ophthalmol Vis Sci*. 2013;54:3463–3471.
20. Kim JS, Ishikawa H, Gabriele ML, et al. Retinal nerve fiber layer thickness measurement comparability between time domain optical coherence tomography (OCT) and spectral domain OCT. *Invest Ophthalmol Vis Sci*. 2010;51:896–902.
21. Latrive A, Boccara AC. In vivo and in situ cellular imaging full-field optical coherence tomography with a rigid endoscopic probe. *Biomed Opt Exp*. 2011;2:2897–2904.
22. Xiao P, Fink M, Boccara AC. Transmission Glass-Like Aberrations Correction for Full-Field OCT Imaging. *Imaging and Applied Optics 2015*. OSA Technical Digest (online) (Optical Society of America, 2015), paper AOTh3D.4. Available at: https://www.osapublishing.org/abstract.cfm?uri=AOMS-2015-AOTh3D.4. Accessed April 1, 2016.
23. Dubra A, Sulai Y, Norris JL, et al. Noninvasive imaging of the human rod photoreceptor mosaic using a confocal adaptive optics scanning ophthalmoscope. *Biomed Opt Exp*. 2001;2:1864–1876.
24. Berger A, Cavallero S, Dominguez E, et al. Spectral-domain optical coherence tomography of the rodent eye: highlighting layers of the outer retina using signal averaging and comparison with histology. *PLoS One*. 2014;9:e96494.
25. Spaide RF, Curcio CA. Anatomical correlates to the bands seen in the outer retina by optical coherence tomography: literature review and model. *Retina*. 2011;31:1609–1619.
26. Jonnal RS, Kocaoglu OP, Zawadzki RJ, Lee SH, Werner JS, Miller DT. The cellular origins of the outer retinal bands in optical coherence tomography images. *Invest Ophthalmol Vis Sci*. 2014;55:7904–7918.

Investigative Ophthalmology & Visual Science